Electronic Supplementary Information

# Born liquid to live solid: *in situ* polymerized electrolyte enables stable operation of organic - Li metal batteries

Guzaliya R. Baymuratova,[a] Elena V. Shchurik,[a] Nikita A. Emelianov,[a] Alexander V. Mumyatov,[a] Ivan S. Zhidkov,[b,c] Alexander F. Shestakov,[a,d] Olga V. Yarmolenko,[a] Olga A. Kraevaya*[a] and Pavel A. Troshin*[e,a]

[a.] *Federal Research Center of Problems of Chemical Physics and Medicinal Chemistry RAS, Semenov Prospect 1, 142432, Chernogolovka, Moscow region, Russian Federation.*

[b.] *Institute of Physics and Technology, Ural Federal University, 620002 Yekaterinburg, Russian Federation.*

[c.] *M. N. Mikheev Institute of Metal Physics of Ural Branch of Russian Academy of Sciences, 620108 Yekaterinburg, Russian Federation.*

[d.] *Department of Fundamental Physics & Chemical Engineering, M.V. Lomonosov Moscow State University, Leninskie Gory 1/51, 119991, Moscow, Russian Federation.*

[e.] *Zhengzhou Research Institute of HT, Longyuan East 7th 26, Jinshui District, 450003, Zhengzhou, China.*

## Table of contents

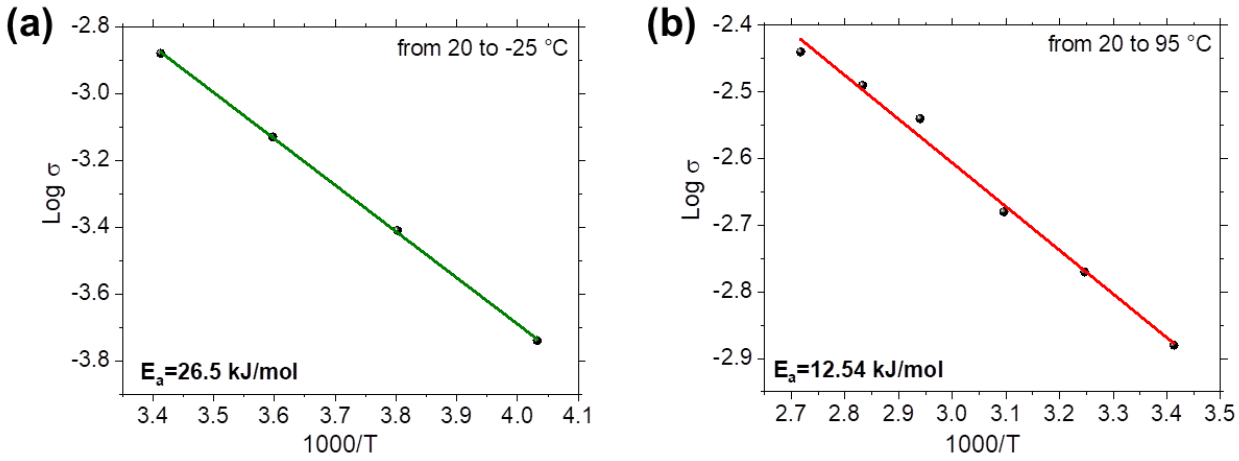


Figure S1. Arrhenius dependence of the conductivity from the inverse temperature dependence in the range of -25-20 °C (a) and 20-95 °C (b) for GPE-based electrolyte.

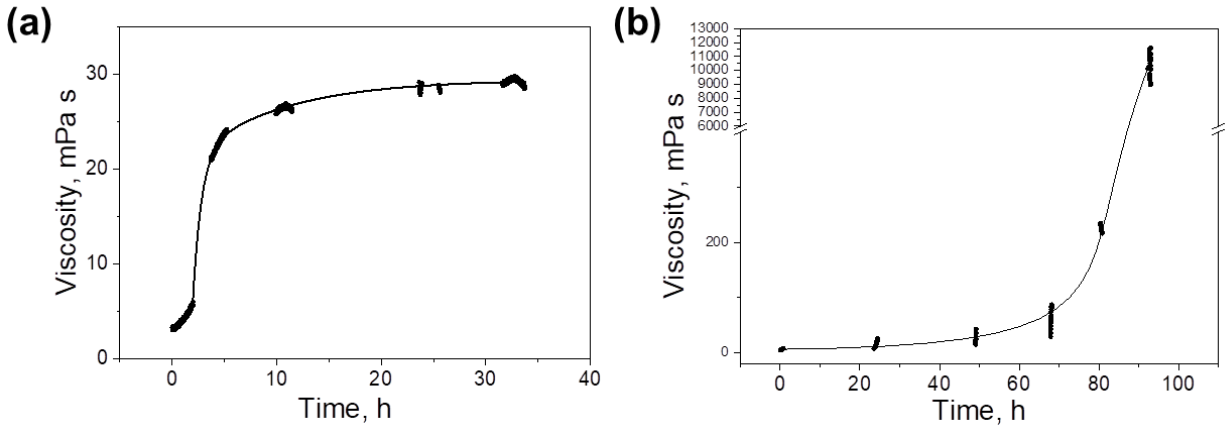


Figure S2. Dynamic viscosity versus time for DOL-based GPE (a) and carbonate-free LiTFSI/$LiPF_6$/DOL/DME at 25 ºC.

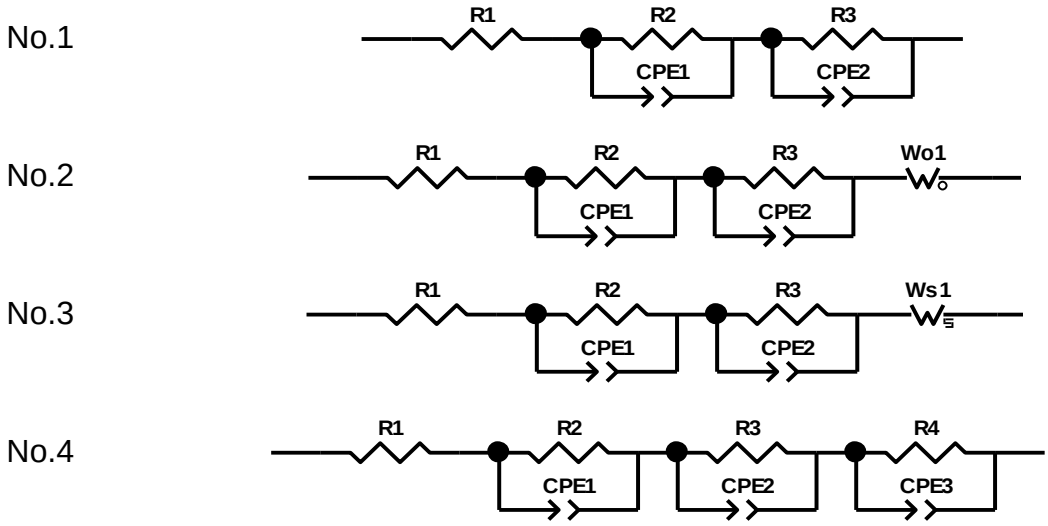


Figure S3. Equivalent circuits for Nyquist plots, where R1 is the electrolyte resistance, R2 is the resistance at the electrode/electrolyte interface; CPE is the Constant Phase Element; W is Warburg diffusion coefficient (o – open, s – short).

Table S1. Calculated parameters of equivalent cell circuits

| | Symmetrical cells | | Delithiation | | Lithiation | | |
|---|---|---|---|---|---|---|---|
| | Li // Li | **PTPQ//PTPQ** | Li // **PTPQ** (0.7V) | Li // **PTPQ** (2.5V) | Li // **PTPQ** (0.5V) | | Li // **PTPQ** (1.1V) |
| No. eq. circuits | **1** | **2** | **1** | **3** | **1** | | **4** |
| R1 | 1.7 | 2.2 | 6.8 | 8.8 | 8 | R1 | 9.4 |
| R2 | 4.8 | 4.3 | 27 | 20 | 21 | R2 | 14 |
| CPE1-T | $1.4\times10^{-6}$ | $1.5\times10^{-7}$ | $7.6\times10^{-5}$ | $9.2\times10^{-6}$ | $2.4\times10^{-5}$ | CPE1-T | $3.3\times10^{-6}$ |
| CPE1-P | 0.81 | 0.97 | 0.47 | 0.65 | 0.56 | CPE1-P | 0.72 |
| R3 | **217** | **9.1** | 172 | 32 | 137 | R3 | 33 |
| CPE2-T | $2.8\times10^{-6}$ | $4.1\times10^{-6}$ | $1.4\times10^{-4}$ | $2\times10^{-4}$ | $1.8\times10^{-4}$ | CPE2-T | $5.1\times10^{-5}$ |
| CPE2-P | 0.88 | 0.98 | 0.67 | 0.7 | 0.62 | CPE2-P | 0.98 |
| Wo1-R | - | 18.5 | - | 141* | - | R4 | 364 |
| Wo1-T | - | 0.011 | - | 0.76* | - | CPE3-T | 0.0021 |
| Wo1-P | - | 0.44 | - | **0.43*** | - | CPE3-P | 0.38 |

*-Warburg Short

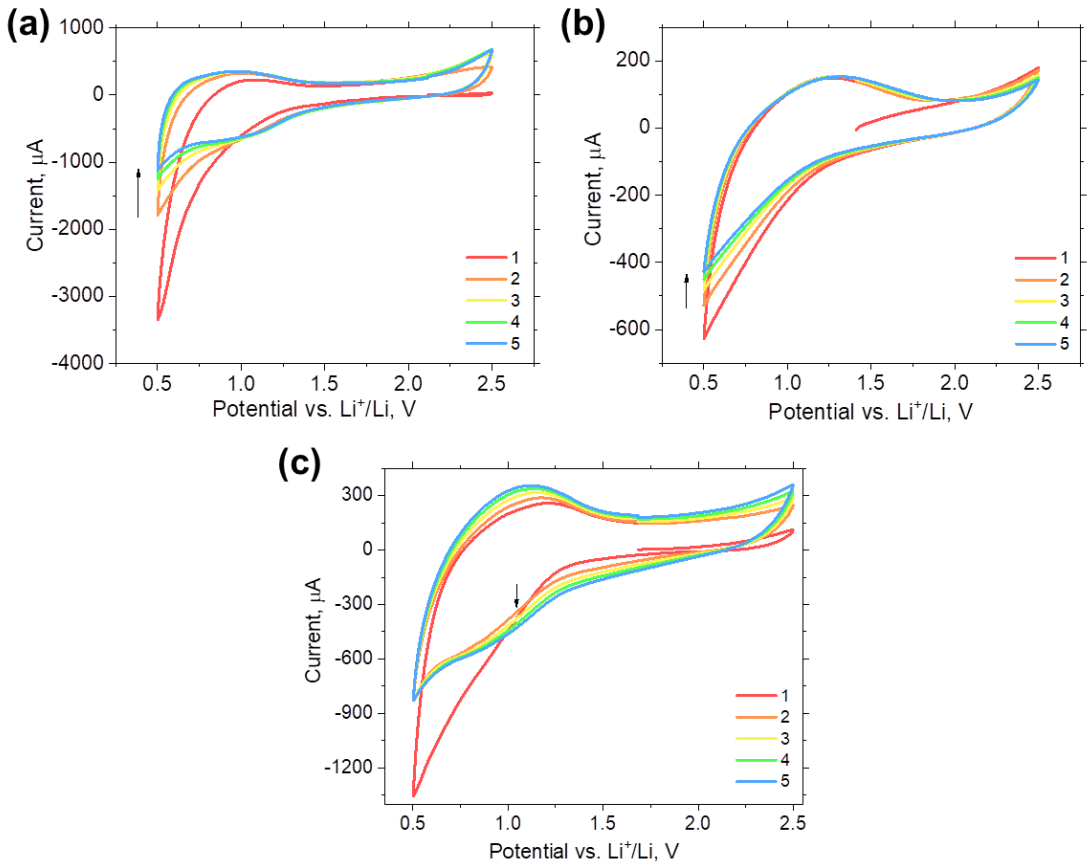


Figure S4. CV profiles for Li/electrolyte/**PTPQ** cells with 1M $LiPF_6$ in EC/DMC (a); 1 M LiTFSI in DOL/DME (b) and *in situ* gelled electrolyte (c) in a potential range of 0.5–2.5 V vs. $Li^+/Li$ (scan rate: 1 mV $s^{-1}$).

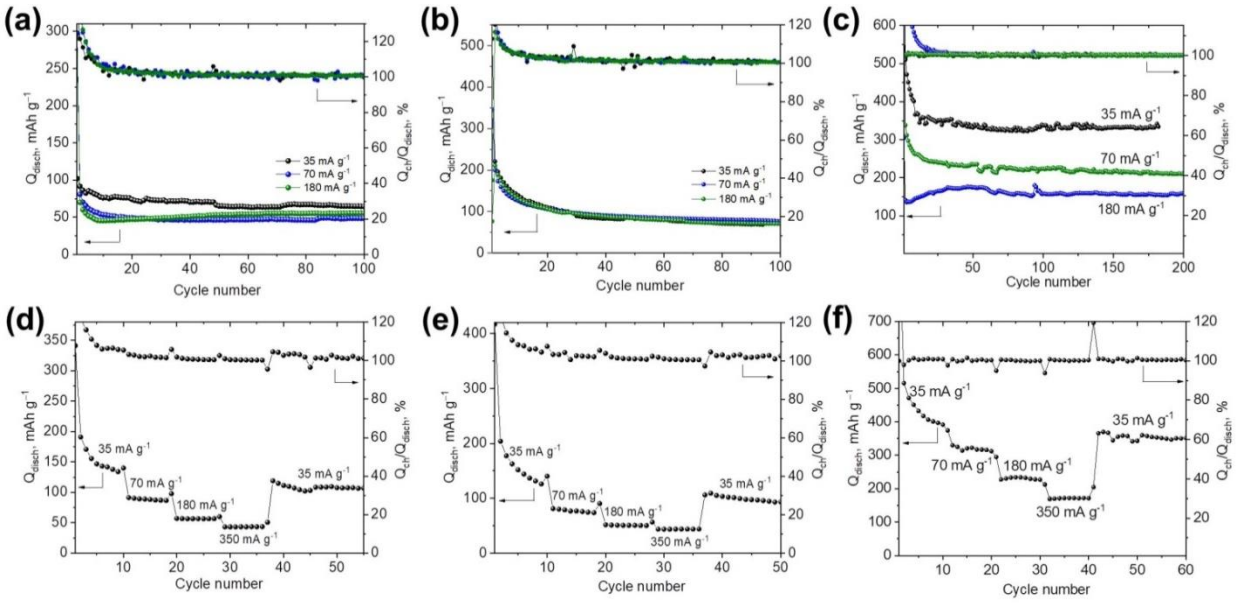


Figure S5. Discharge specific capacities and Coulombic efficiencies of Li/electrolyte/**PTPQ** cells with 1M $LiPF_6$ in EC/DMC (a, d), 1M LiTFSI in DOL/DME (b, e), and DOL-based gel-polymer electrolytes (c, f) during cycling at different current densities within a potential range of 0.5–2.5 V vs. $Li^+$/Li.

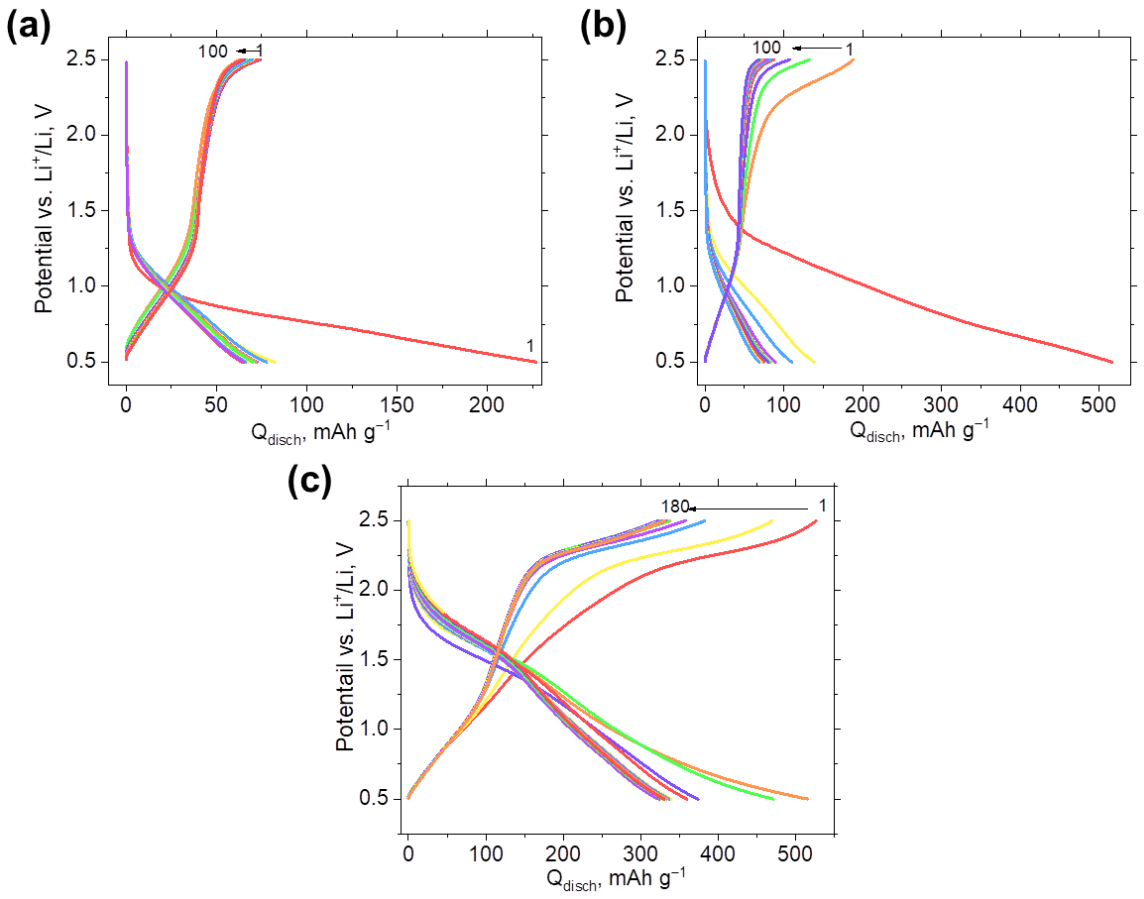


Figure S6. Charge-discharge profiles for Li/electrolyte/**PTPQ** cells with 1M $LiPF_6$ in EC/DMC (a); 1M LiTFSI in DOL/DME (b) and DOL-based GPE (c) in a potential range of 0.5–2.5 V vs. $Li^+/Li$ at the current rate of 35 mA $g^{-1}$.

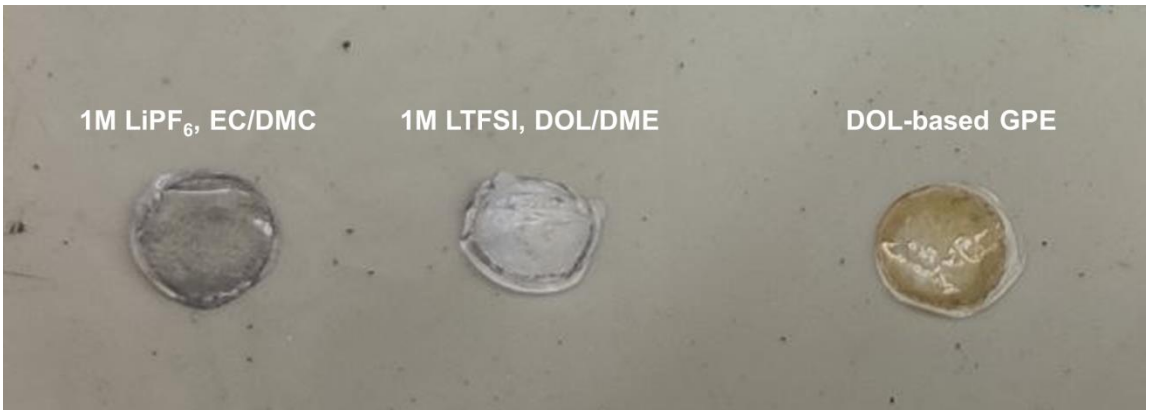


Figure S7. Photographs of the separators extracted from the Li/electrolyte/**PTPQ** cells cycled with different electrolytes (for the liquid electrolytes, traces of dissolved **PTPQ** cathode material are visible (black coloration), and for GPE-based cells, yellowish color is for the polymer electrolyte attached to the separator).


Figure S8. **PTPQ** powder after long-time treatment with various electrolytes.

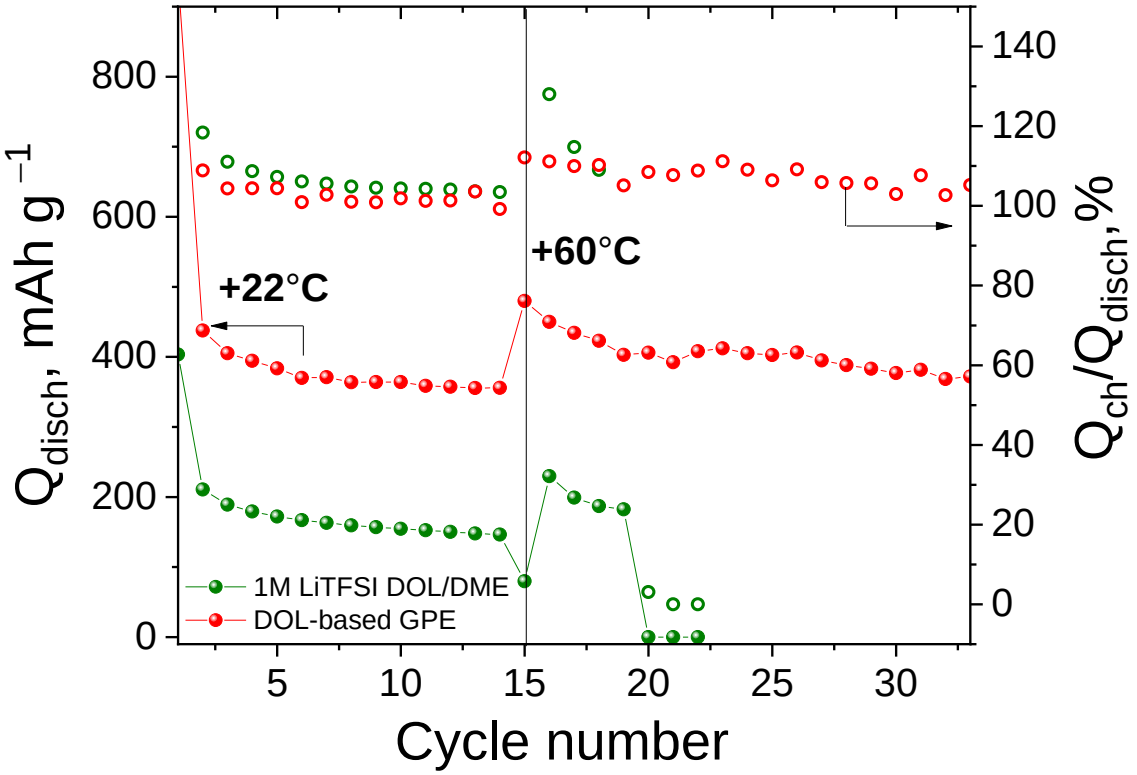


Figure S9. The evolution of the discharge specific capacity and Coulombic efficiency of the Li//**PTPQ** cells with liquid and gelled electrolytes at 22 $^{o}$C and 60 °C when cycled at the current density of 35 mAh g$^{-1}$.

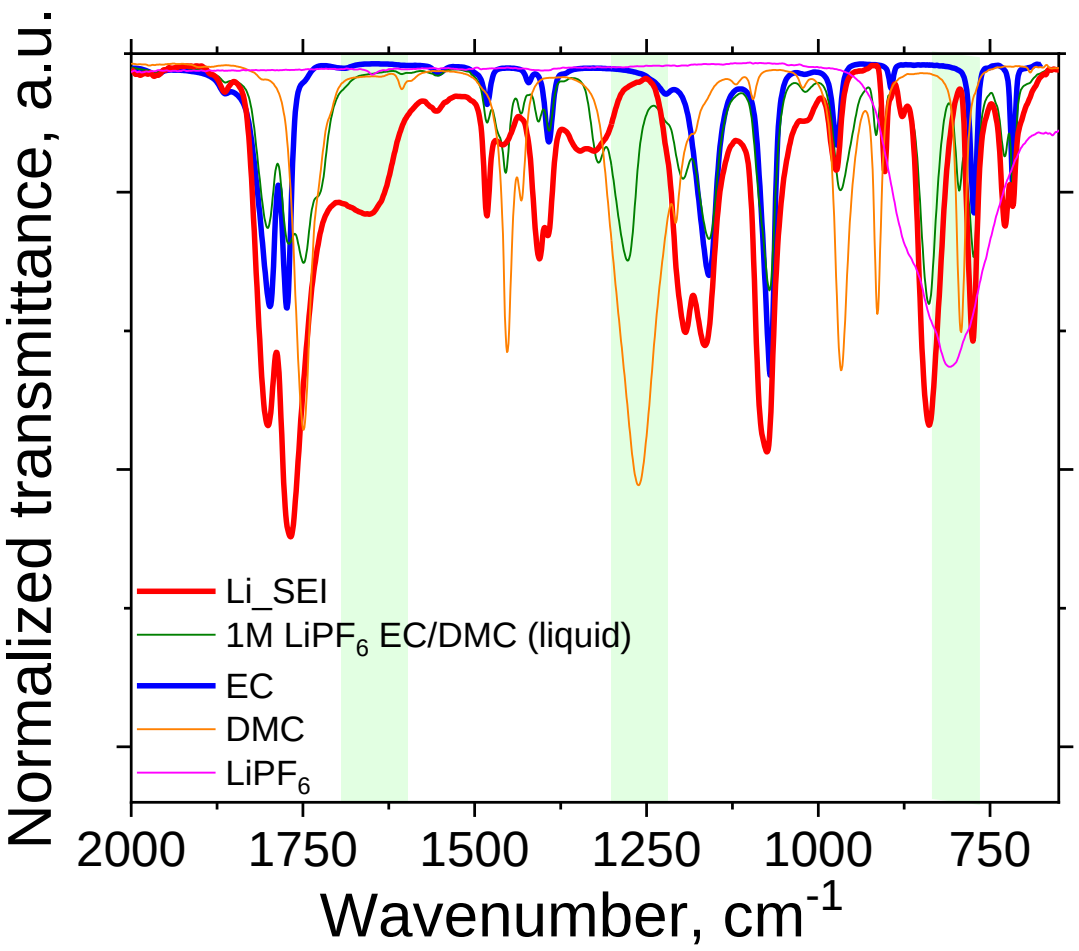


Figure S10. FTIR spectra of Li anodes extracted from the Li//**PTPQ** cells with 1M $LiPF_6$ in EC/DMC electrolytes (Li_SEI), liquid electrolyte and electrolyte components.

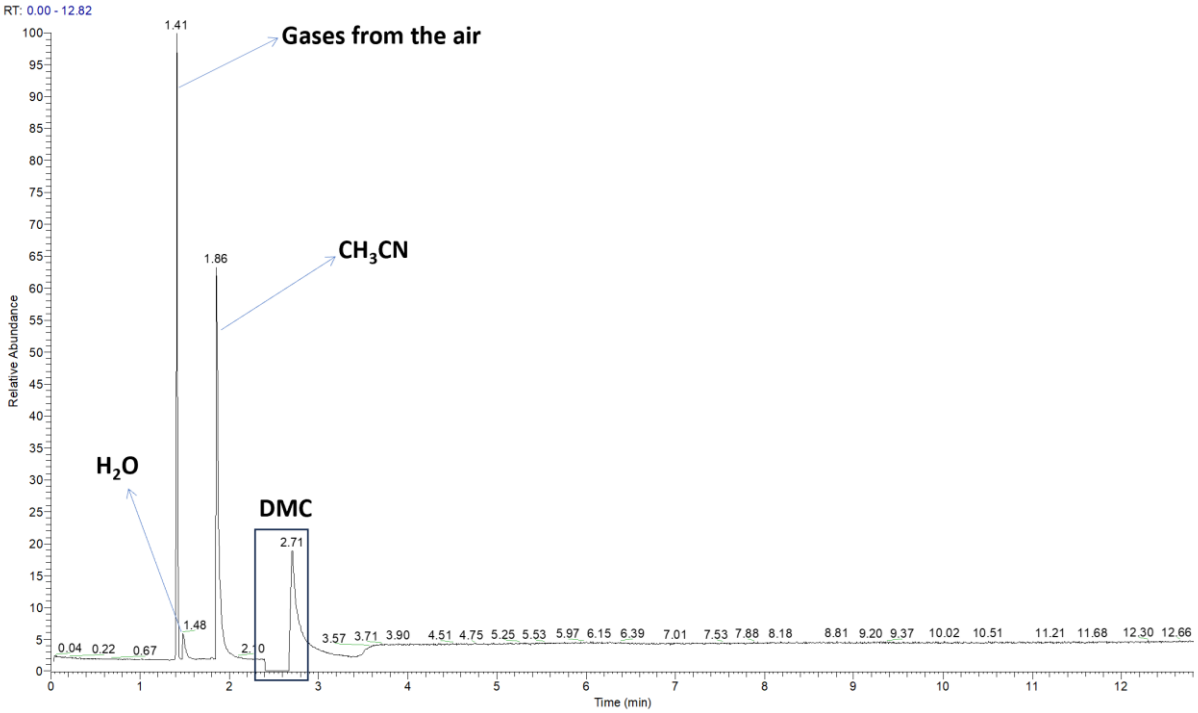


Figure S11. Chromatogram of products of lithium interaction with DMC.

**(a)**

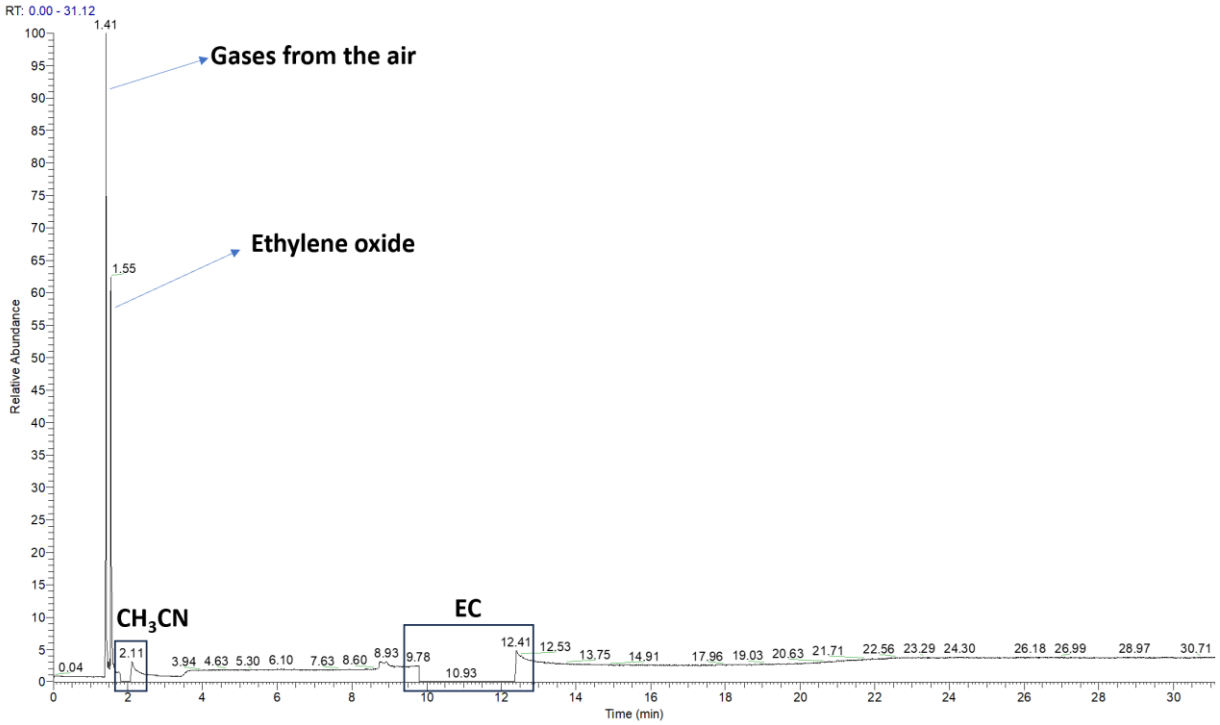


**(b)**

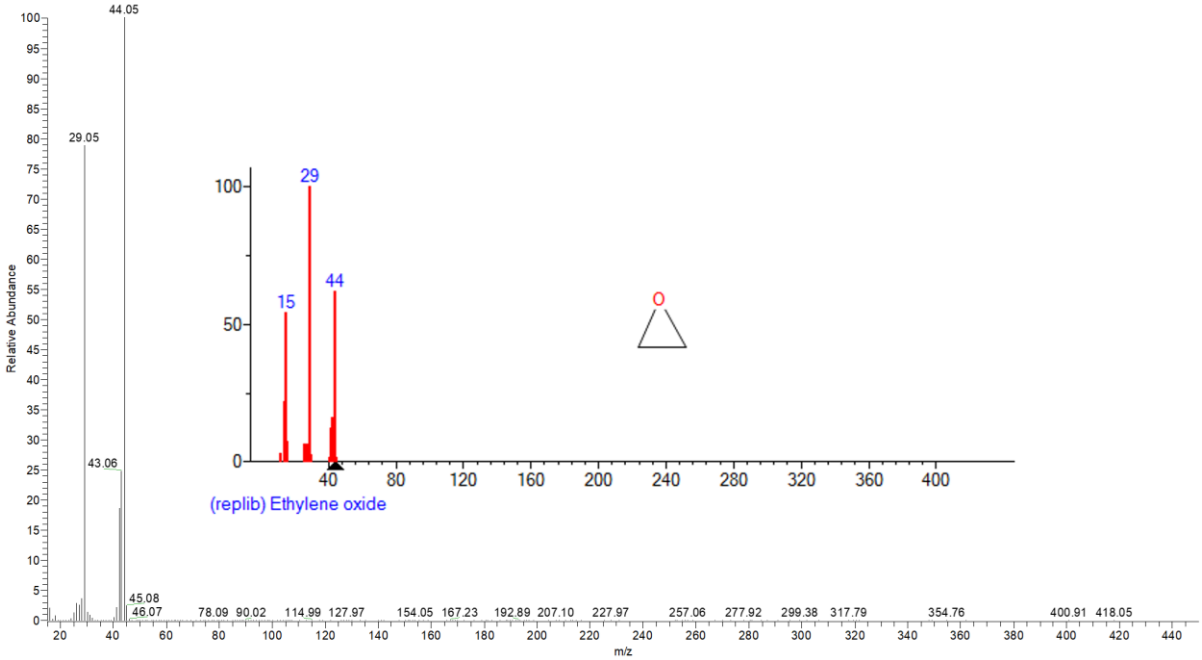


Figure S12. Chromatogram of products of lithium interaction with EC (a) and a mass spectrum of ethylene oxide (b).

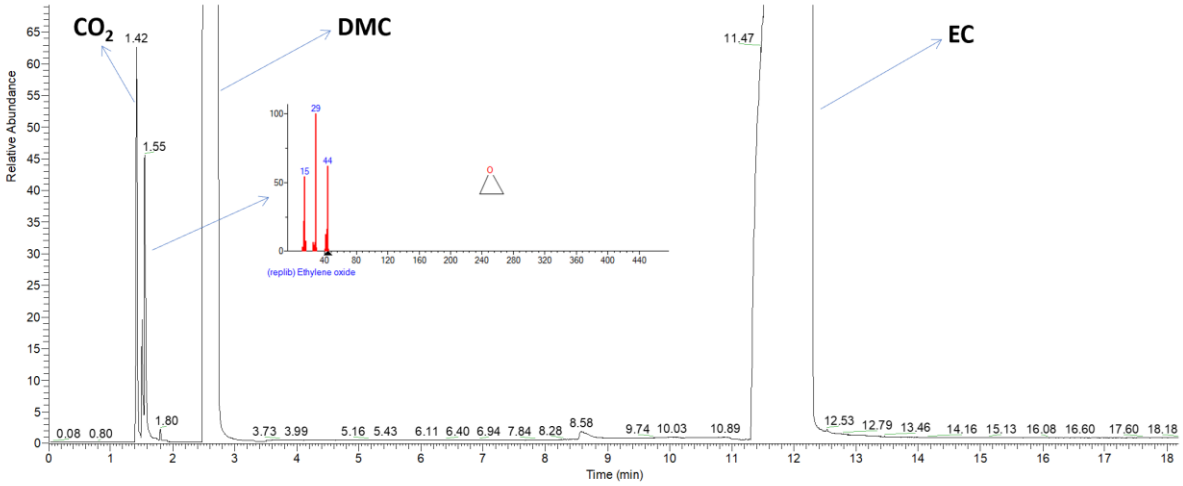


Figure S13. Chromatogram of products of lithium interaction with EC/DMC (1:1 V:V).

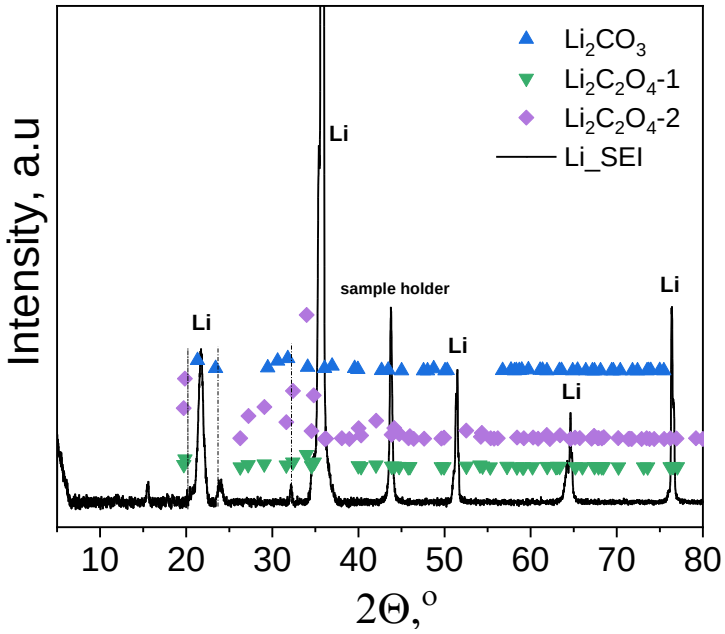


Figure S14. Results of XRD for the Li anodes cycled in the cells with 1M $LiPF_6$ EC/DMC electrolyte and its comparison with the literature data for lithium carbonate and oxalate.

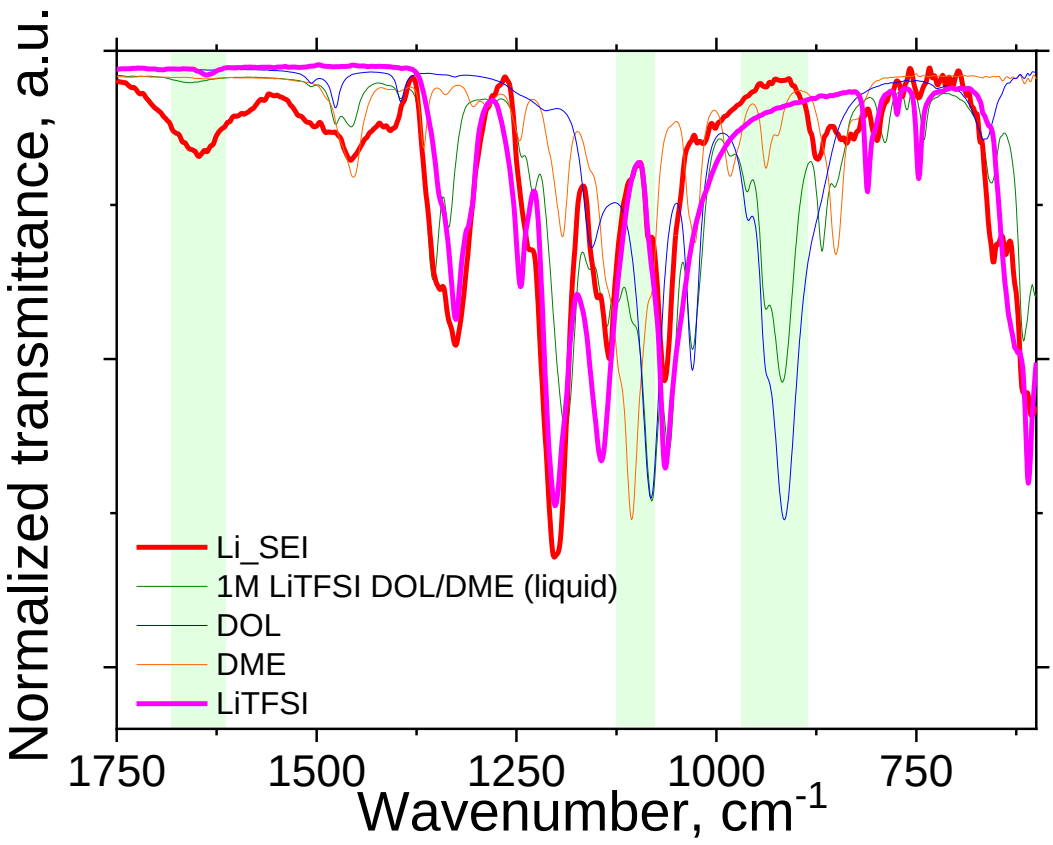


Figure S15. FTIR spectra of Li anodes extracted from the Li//**PTPQ** cells with 1M LiTFSI in DOL/DME electrolytes (Li_SEI), liquid electrolyte and electrolyte components.

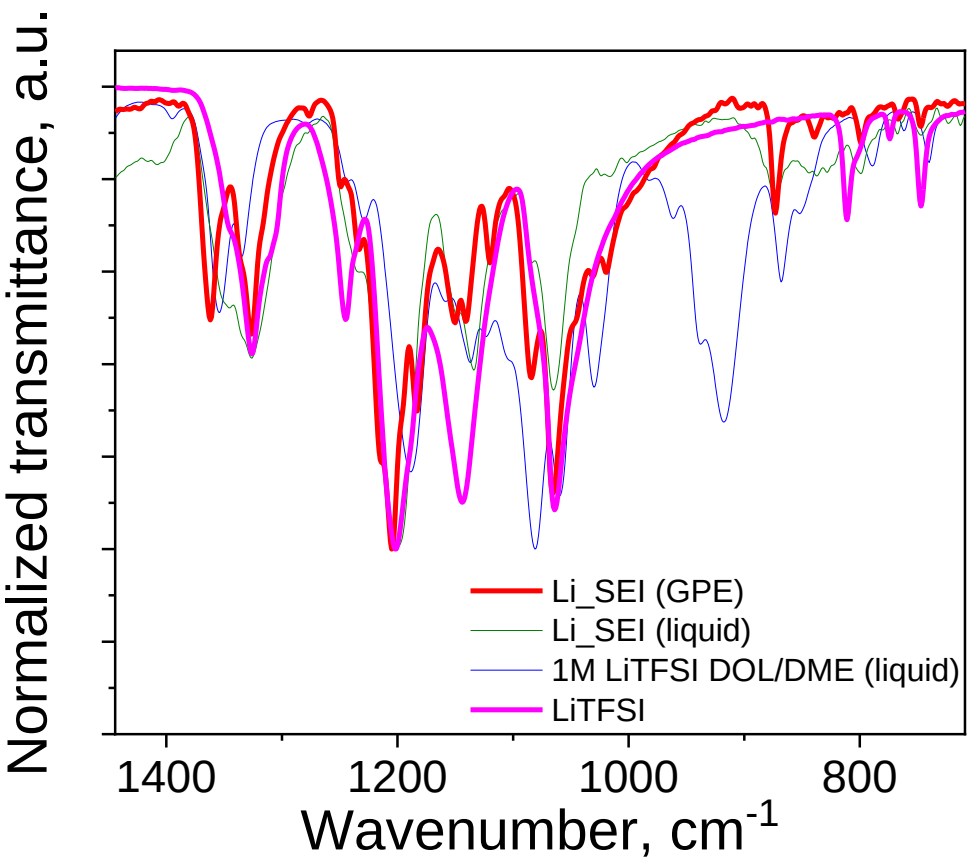


Figure S16. FTIR spectra of Li anodes extracted from the Li//**PTPQ** cells with gel-polymer electrolyte (Li_SEI (GPE)), 1M LiTFSI in DOL/DME electrolyte (Li_SEI (liquid)), liquid electrolyte and LiTFSI.

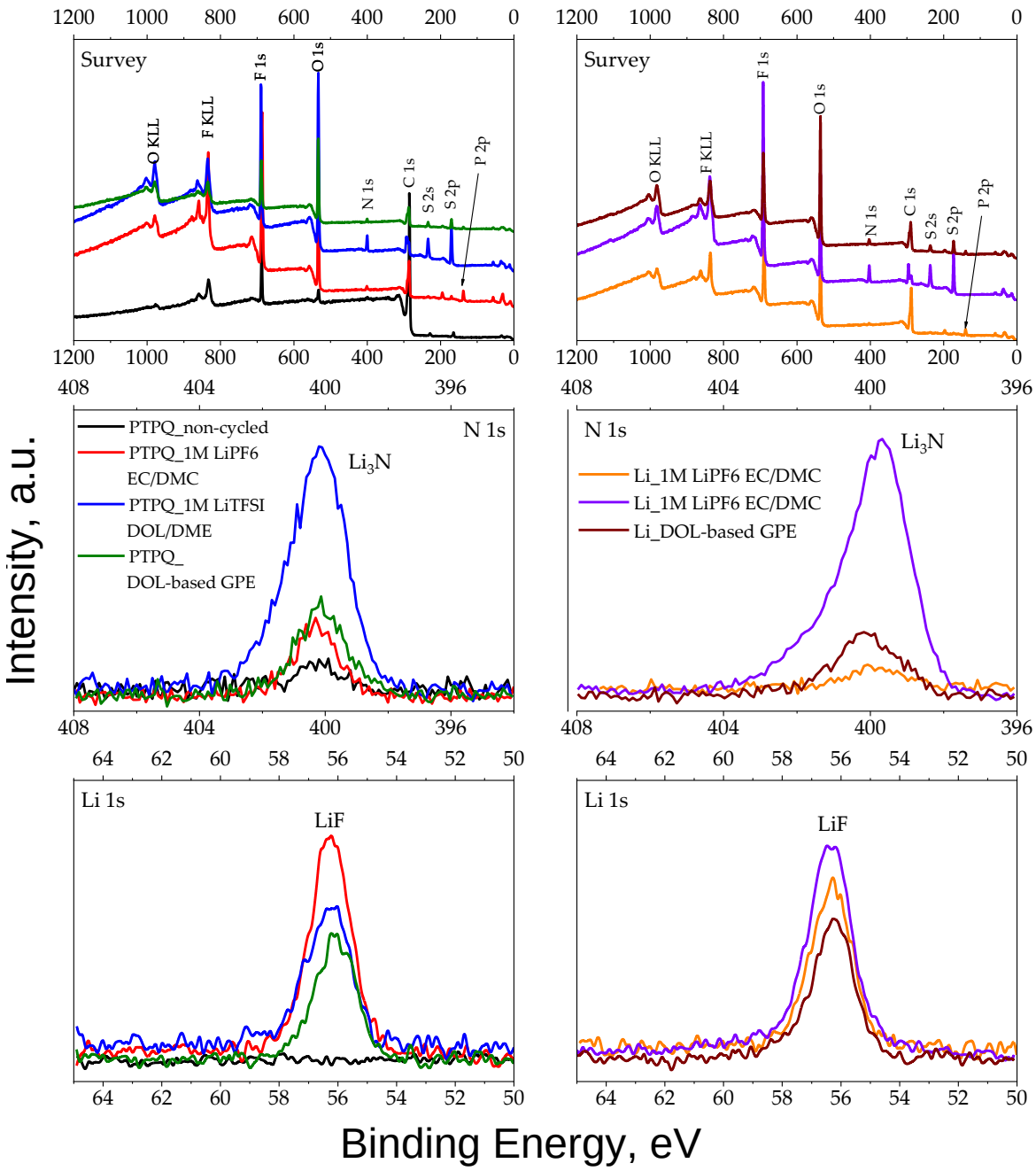


Figure S17. XPS survey and high-resolution N 1s and Li 1s spectra for the **PTPQ** cathode and Li anode extracted from the cells with 1M $LiPF_6$ EC/DMC, 1M LiTFSI DOL/DME and DOL-based GPE electrolytes.

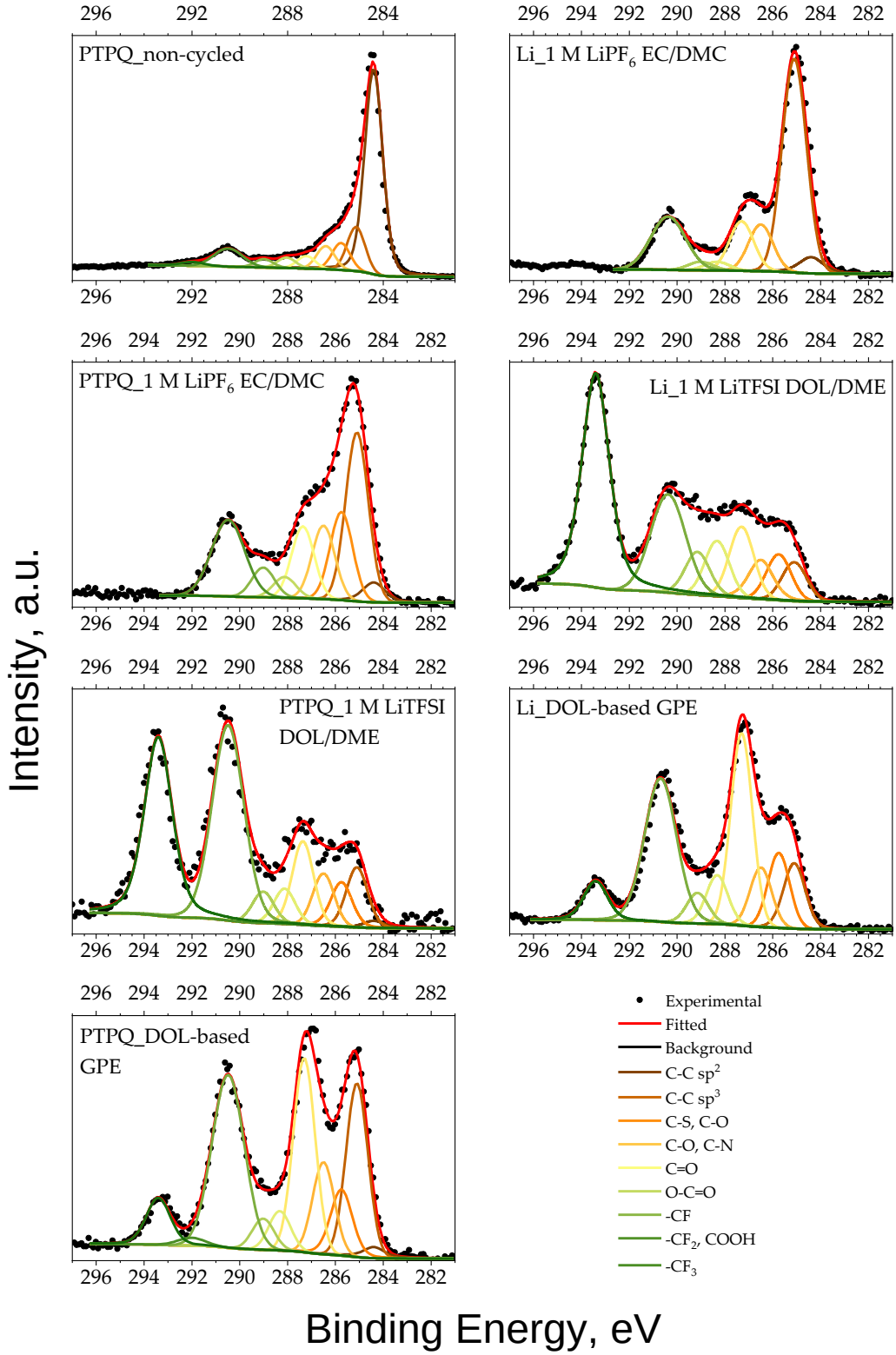


Figure S18. XPS C 1s spectra for the **PTPQ** cathode and Li anode extracted from the cells with 1M $LiPF_6$ EC/DMC, 1M LiTFSI DOL/DME and DOL-based GPE electrolytes.

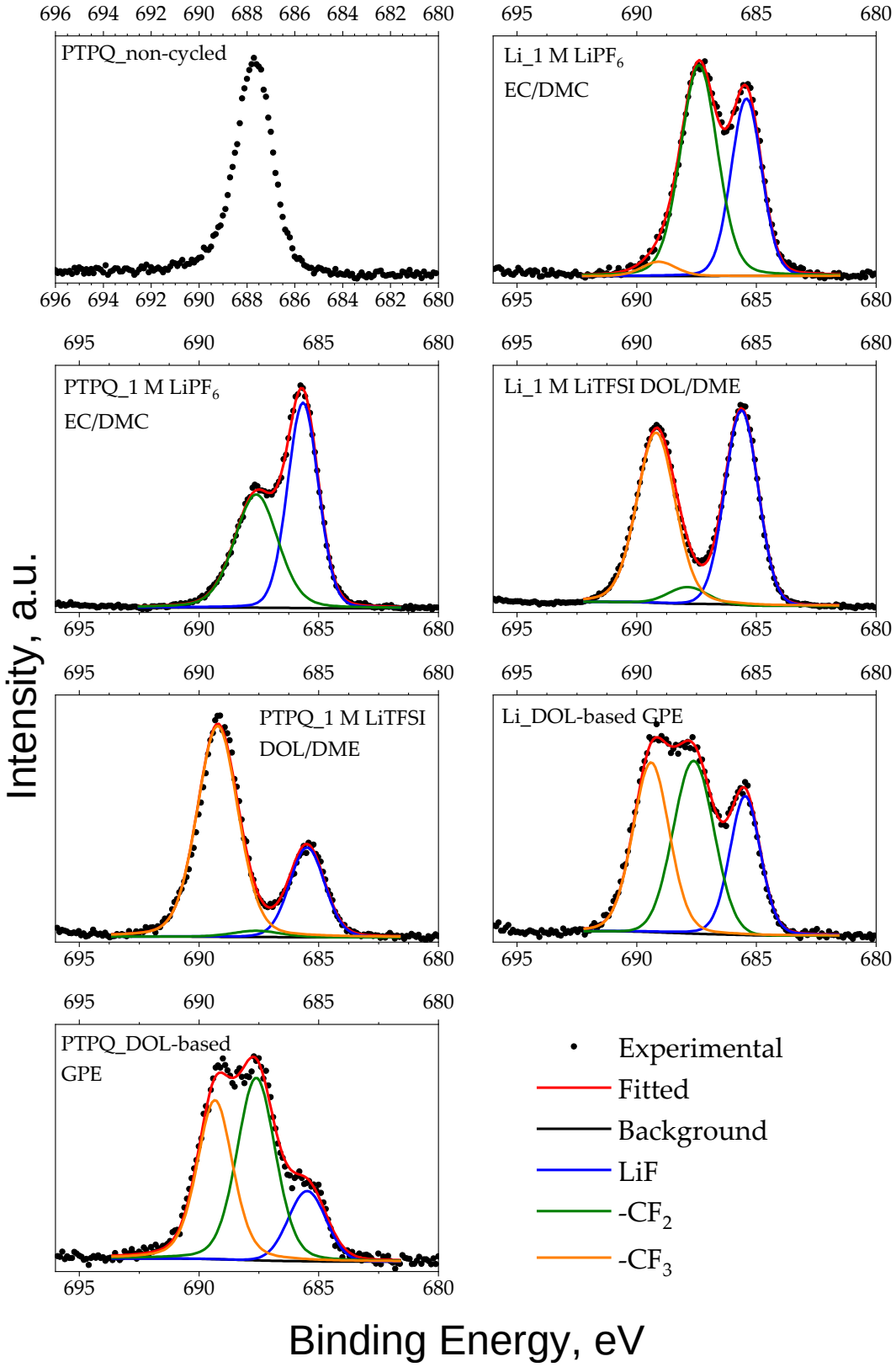


Figure S19. XPS F 1s spectra for the **PTPQ** cathode and Li anode extracted from the cells with 1M $LiPF_6$ EC/DMC, 1M LiTFSI DOL/DME and DOL-based GPE electrolytes.

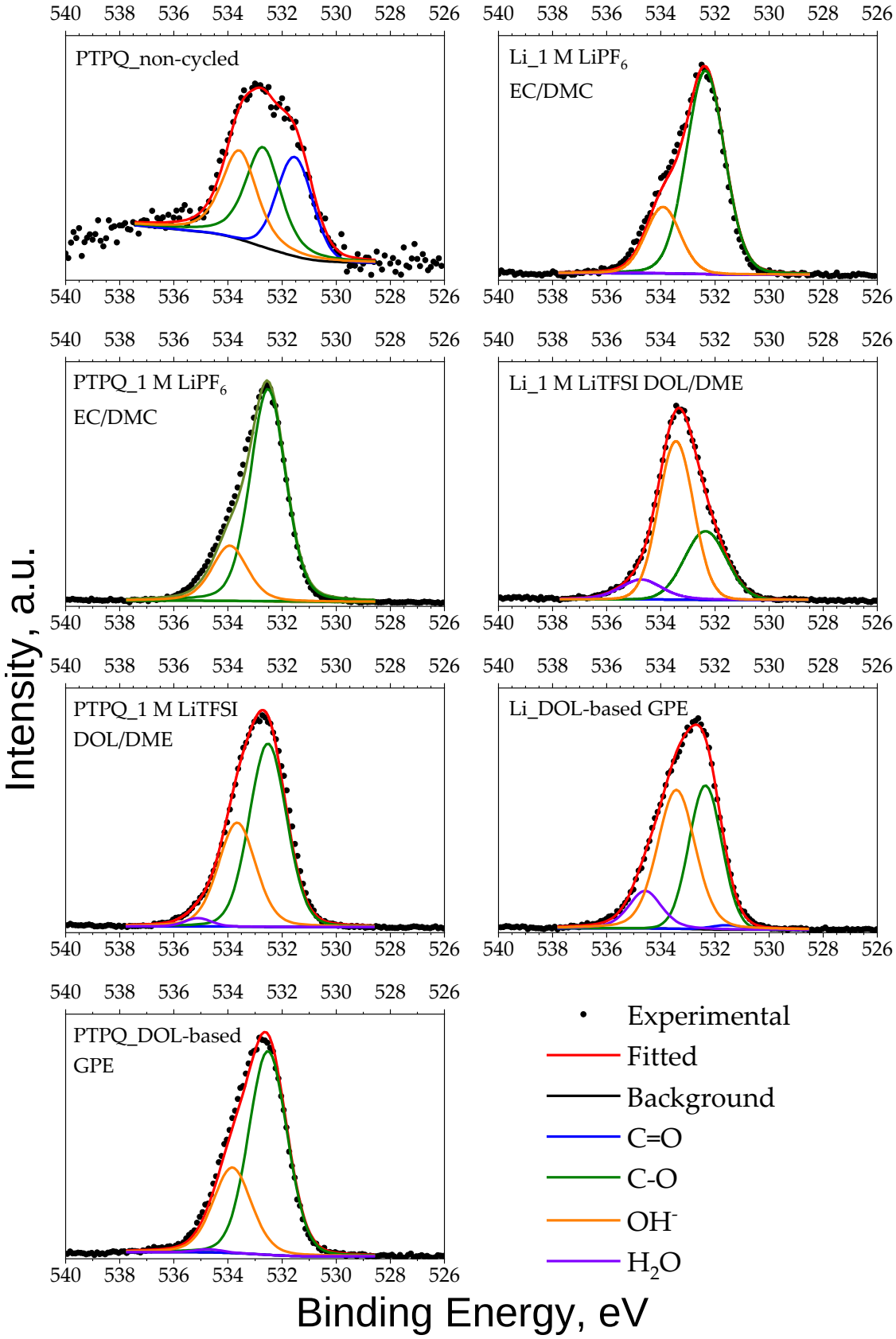


Figure S20. XPS O 1s spectra for the **PTPQ** cathode and Li anode extracted from the cells with 1M $LiPF_6$ EC/DMC, 1M LiTFSI DOL/DME and DOL-based GPE electrolytes.

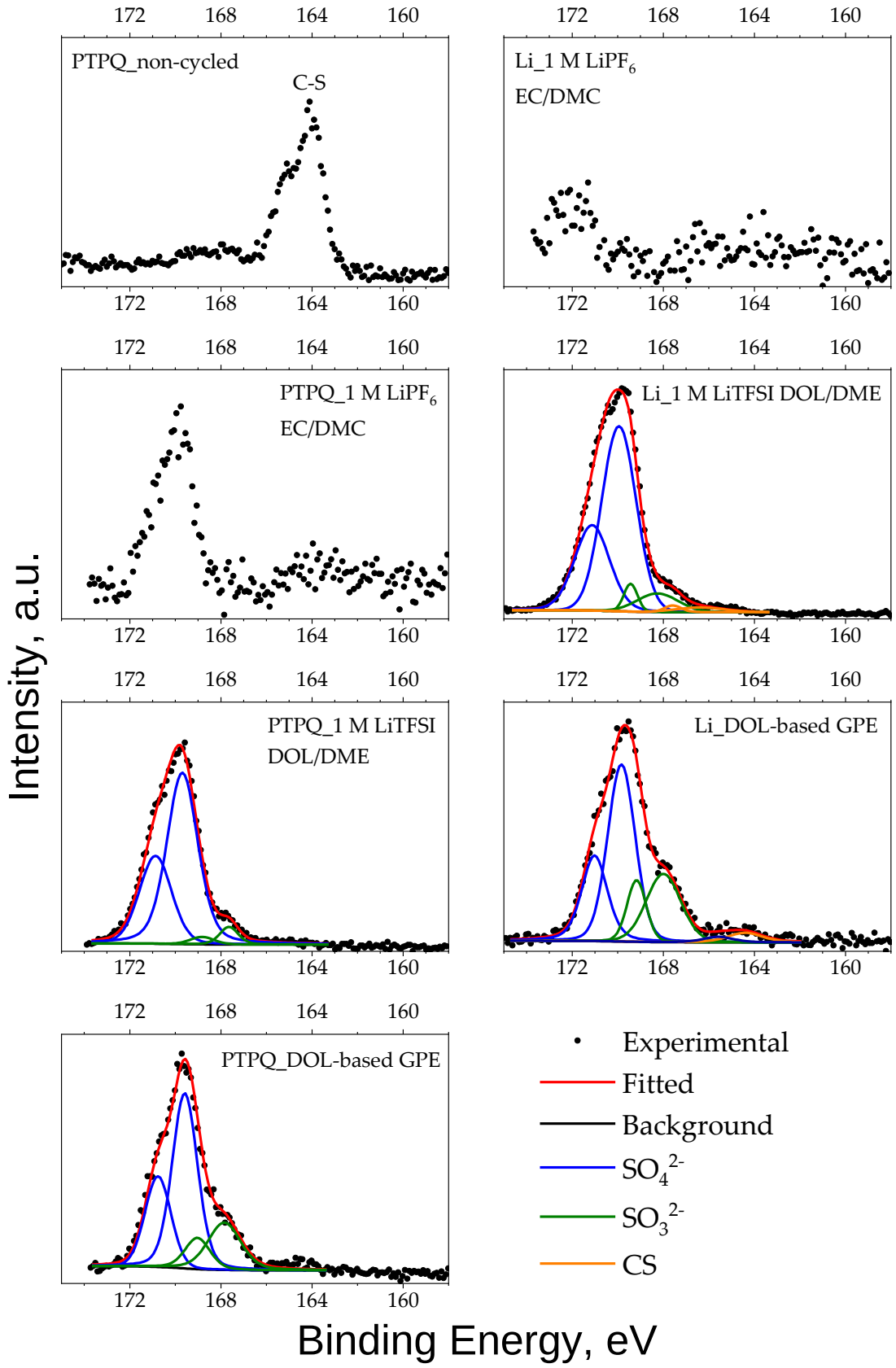


Figure S21. XPS S 2p spectra for the **PTPQ** cathode and Li anode extracted from the cells with 1M $LiPF_6$ EC/DMC, 1M LiTFSI DOL/DME and DOL-based GPE electrolytes.

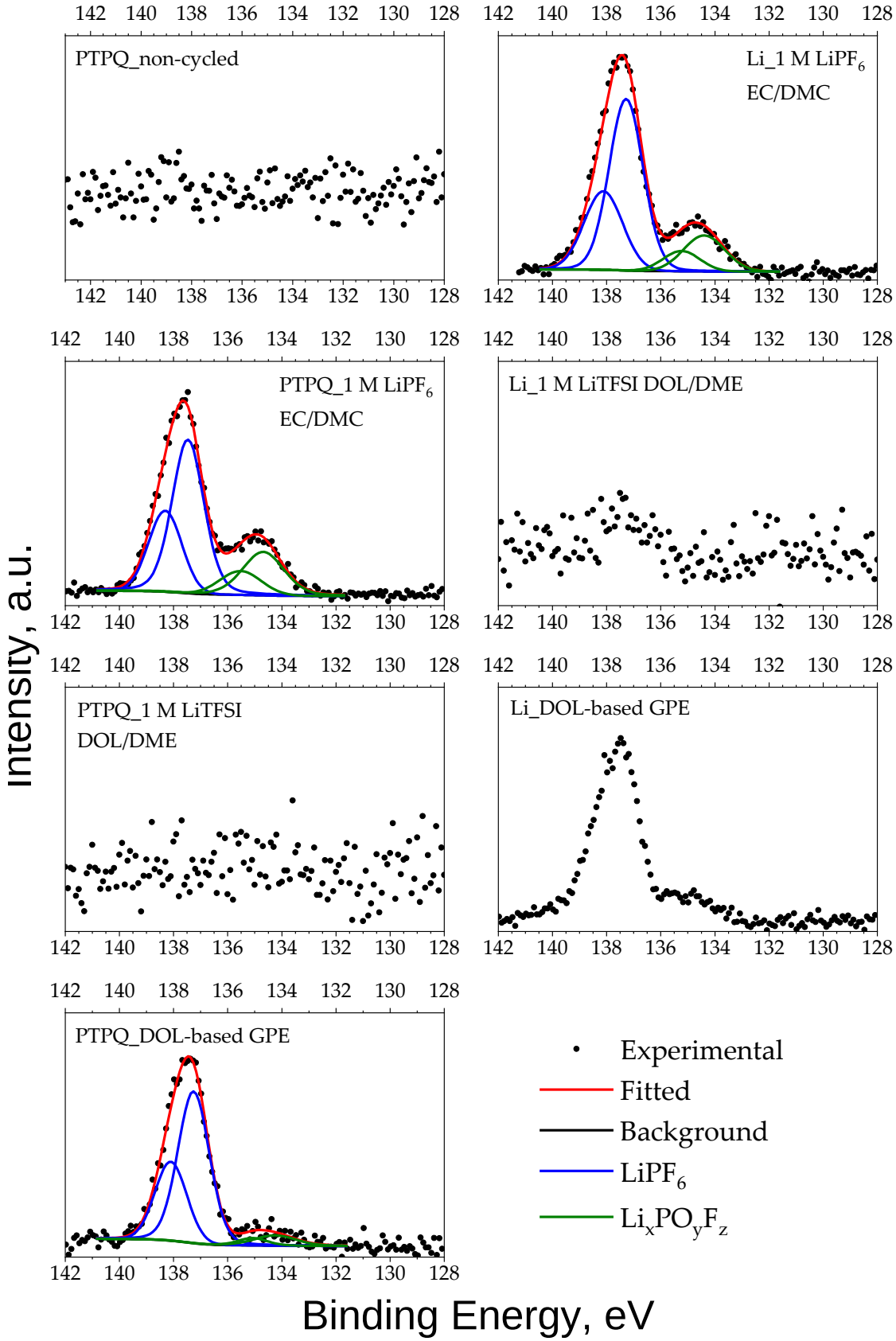


Figure S22. XPS P 2p spectra for the **PTPQ** cathode and Li anode extracted from the cells with 1M $LiPF_6$ EC/DMC, 1M LiTFSI DOL/DME and DOL-based GPE electrolytes.

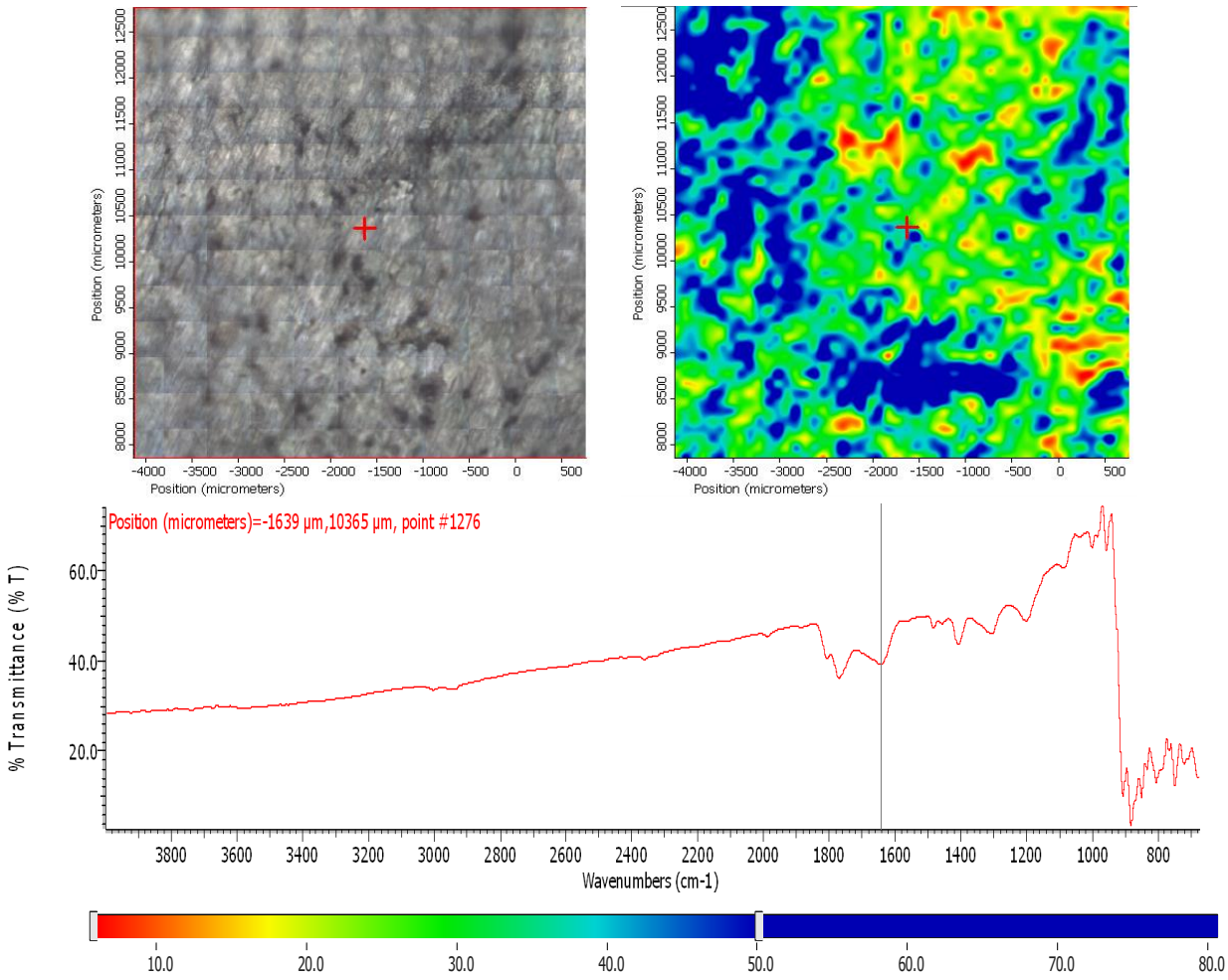


Figure S23. Results of FTIR microscopy for the Li anodes cycled in 1M $LiPF_6$ in EC/DMC: optical image (pixel size100x100 µm, image size 50x50 pixels) and transmittance at 1640 $cm^{-1}$.

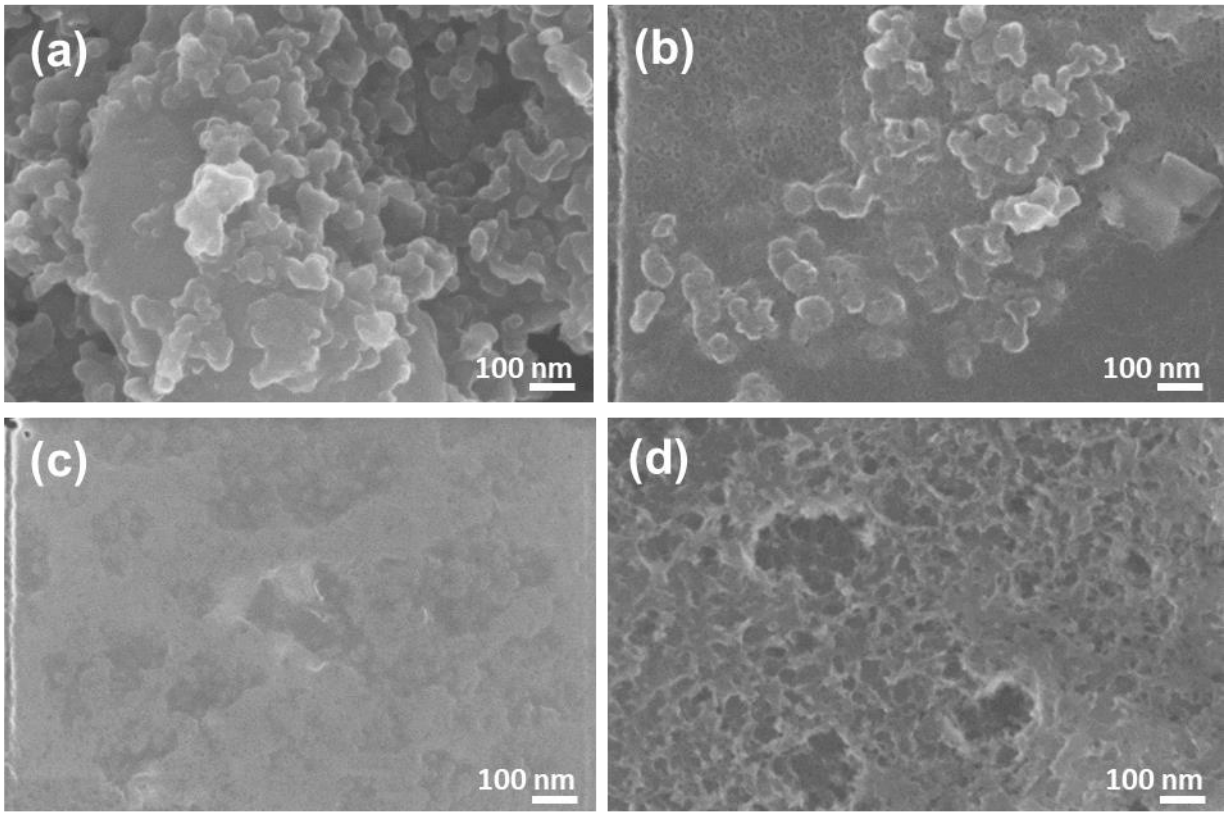


Figure S24. SEM image of organic cathode before cycling (a), extracted from the cells with 1M $LiPF_6$ EC/DMC (b), 1M LiTFSI in DOL/DME (c) and DOL-based GPE (d).

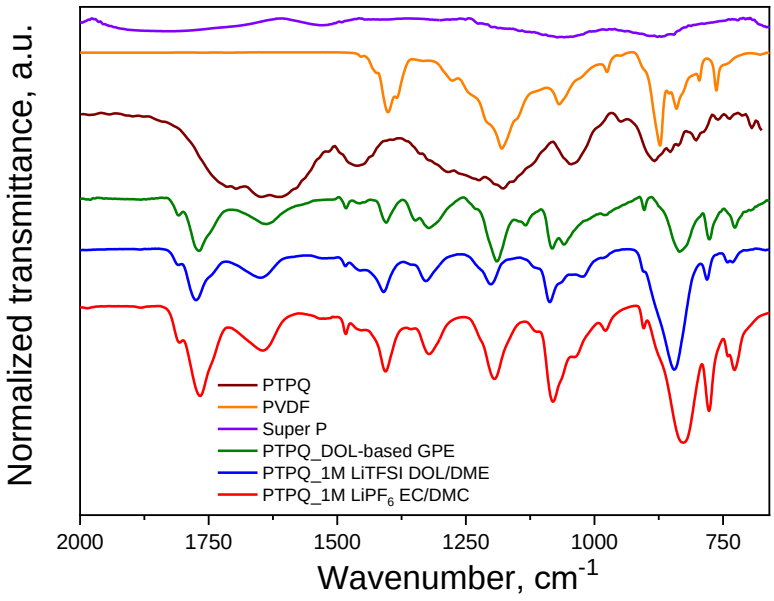


Figure S25**.** FTIR spectra of organic cathode before cycling, extracted from the cells with 1M LiPF6 EC/DMC, 1M LiTFSI in DOL/DME and DOL-based GPE.